Volatile Organic Compound Detection Using Insect Odorant-Receptor Functionalised Field-Effect Transistors

by

Eddyn Oswald Perkins Treacher

A thesis submitted in fulfilment of the
requirements of the degree of
Doctor of Philosophy in Physics
School of Physical and Chemical Sciences
Te Herenga Waka - Victoria University of Wellington

Aug 2023

Acknowledgements

Thanks for all the fish.

Abstract

This is a thesis skeleton written with quarto. Make a copy of this thesis repo and start to write!

Make a new paragraph by leaving a blank line.

Table of contents

1. Introduction

This is a book created from markdown and executable code.

See for additional discussion of literate programming.

```
[1] 2
```

2. Carbon Nanotube and Graphene Field-Effect Transistors

2.1. Device Functionalisation

2.2. Insect Odorant Receptors

3. Carbon Nanotube and Graphene Field-Effect Transistors as Biosensor Platforms

4. Fabrication of Carbon Nanotube Network and Graphene Field-Effect Transistors

This chapter discusses the fabrication processes for both the carbon nanotube network and graphene transistors. Experimental optimisation of the transducer element is critical for biosensor work, and large numbers of transducers were required for testing various biosensor functionalisation processes. Therefore, these processes were developed to rapidly fabricate devices with reproducible device characteristics appropriate for biosensing work. Also outlined in this chapter are the characterisation techniques taken to test the quality and reproducibility of these fabrication processes.

The nitrogen ($\geq$ 99.99%) and oxygen (99.7%) used in fabrication work was supplied by BOC Limited New Zealand. Deionised (DI) water was taken from a Synergy® UV Water Purification System. The DI water had a measured conductivity of (1.4 ± 0.1) μS cm^{-1}, compared to tap water with a measured conductivity of (7.8 ± 0.2) μS cm^{-1}.

4.1. Deposition of Carbon Nanotubes

4-inch *p*-type (B-doped) silicon wafers with either a 100 nm or 300 nm SiO_2 layer (WaferPro LLC) were used as the substrate for carbon nanotube network deposition. A 100 nm SiO_2 layer was the preferred option for the devices intended for backgated measurements. Before deposition of carbon nanotubes, the wafers were spin-coated with AZ® 1518 photoresist, placed photoresist-side down onto a cleanroom wipe, fixed in place using vacuum suction, then cleaved into quarters using a diamond-tipped scribe tool. For fabrication performed before June 2023, the protective photoresist layer was then removed by soaking the quarter-wafers in acetone for 15 minutes, then rinsed with isopropyl alcohol (IPA) and dried with N2 gas. However, for complete removal of photoresist, we found it was necessary to flood expose the device with the Karl Suss Aligner for 1 min and then place it in AZ326 developer for 3 min, as discussed further in Section 4.2.

Carbon nanotubes were deposited before alignment markers photolithography on all wafers fabricated between Aug 2021-Feb 2023, while devices fabricated before Aug 2021 and after Feb 2023 had alignment markers photolithography performed before the deposition of carbon nanotubes. The process order was first switched in Aug 2021 as successive

deposition of carbon nanotubes onto many quarter wafers before the rate-limiting alignment markers step led to faster processing times. However, the order was switched back in Feb 2023 to minimise the exposure of carbon nanotubes to photolithographic chemical processes.

4.1.1. Solvent-Based

The solvent-based deposition process for the carbon nanotube network in the second fabrication protocol is as follows. 10 mg of 2-mercaptopyridine (99%, Sigma-Aldrich) was dissolved in 1 ml ethanol by sonication until clear. Quarter wafers were sonicated in acetone for 3 min, then plasma cleaned for 2 min at 50 W (300 mTorr) in a PE-50 Compact Benchtop Plasma Cleaning System (Plasma Etch, Inc.). The cleaned SiO_2/Si surface was then coated with 2-mercaptopyridine for 10 minutes, rinsed with ethanol to remove residual 2-mercaptopyridine, and then nitrogen dried. Meanwhile, 5 μg of carbon nanotube bucky paper (NanoIntegris, IsoNanotubes S-99) was dispersed in 10 mL of dichlorobenzene (Sigma Aldrich) by ultrasonication until no particles were visible to the naked eye. During this time, the ultrasonic bath temperature was kept between 20 - 30 °C or the buckypaper would not disperse successfully. The substrates were then placed into a dish with CNT-DCB suspension and left covered for 1 hour, dipped into ethanol for 10 min to remove excess solvent and any unattached carbon nanotube bundles, and then dried with nitrogen.

4.1.2. Surfactant-Based

Simple Dropcasting

2 mL of IsoNanotubes-S 90% or 99% solution was decanted into a small bottle and sonicated for 5 s to break up bundles of CNTs. Place an even spread of 400 μL CNT solution across the centre of the devices on the PLL-functionalised quarter wafer, cover and leave for 10 minutes. The CNT solution was then rinsed off with DI water and IPA, and then the quarter wafer was dried with N_2 gas. Next, the quarter wafer was annealed in a vacuum oven at 150°C for 1 hour. This method would often lead to an inhomogeneous spread of CNTs across the quarter wafer surface, detailed further in section Section 4.3.

Steam-assisted Method

2.5 mL of CNT dispersion was decanted into a small bottle and burst-sonicated once (on then off again) to break up bundles of CNTs. 75 mL of 95°C water was then placed into a glass dish on a hotplate held at 95°C. After this, the PLL-functionalised quarter wafer was placed in the centre of a separate, high-walled glass dish and the CNT dispersion was spread across the surface, being careful not to get too close to the edges. The

quarter wafer glass dish was then placed into the 95°C water dish without any of the CNT solution running off the side of the wafer, then both glass dishes were covered and left for 2 minutes. The CNT solution was then rinsed off with DI water and IPA, and then the quarter wafer was dried with N_2 gas. As in the original method, the quarter wafer was then annealed in a vacuum oven at 150°C for 1 hour. This method gave an even spread of CNTs across the quarter wafer surface, leading to a greater consistency in performance between devices.

4.2. Characterisation via Fluorescence Microscopy

4.3. Characterisation via Atomic Force Microscopy

5. Functionalisation of Carbon Nanotubes and Graphene with Odorant Receptors

5.1. Linker molecules

5.1.1. 1-Pyrenebutanoic acid N-hydroxysuccinimide ester (PBASE)

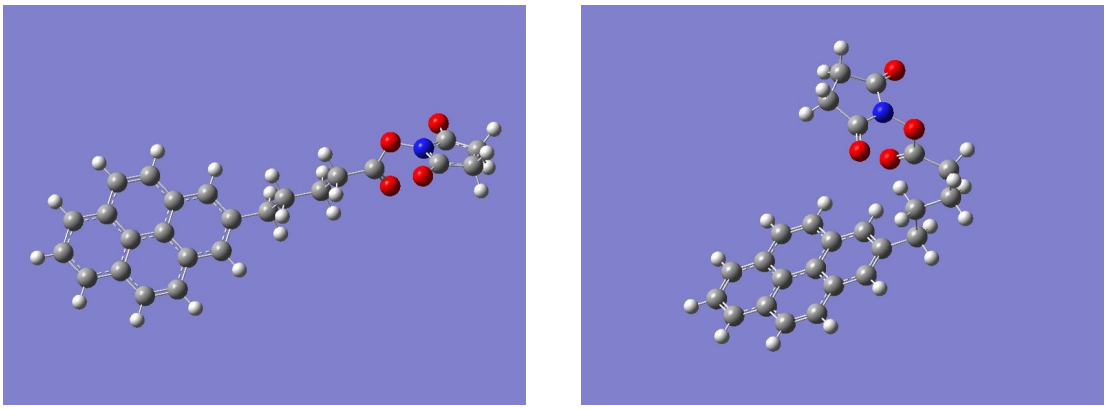

(a) Hartree-Fock energy: -3427728.67 kJ/mol (9 s.f.)

(b) Hartree-Fock energy: -3427729.66 kJ/mol (9 s.f.)

Figure 5.1.: Two conformations of PBASE molecule with geometry optimised via *ab initio* calculation (computed using Gaussian 16 [1]). The difference between computed Hartree-Fock energies is 1.0 kJ/mol, small enough that the existence of both molecular conformations is physically possible.

1-Pyrenebutanoic acid N-hydroxysuccinimide ester (variously known commercially and in the literature as 1-Pyrenebutyric acid N-hydroxysuccinimide ester, PBASE, PBSE, PASE, Pyr-NHS, PyBASE, PANHS) is a aromatic, bifunctional molecule commonly used for tethering biomolecules to the carbon rings of graphene and carbon nanotubes. The optimised molecular structure of PBASE is shown in Figure 5.1.

The non-covalent functionalisation of proteins onto a single-walled carbon nanotube using PBASE was first reported by Chen *et al.* in 2001 [2]. Two methods for protein functionalisation and immobilisation were successfully used, with the only differences being the solvent used to dissolve the PBASE powder (DMF, methanol) and the final

concentration of the resulting solutions (6 mM, 1 mM respectively). The lower concentration may have been used for PBASE in methanol as PBASE powder appears to dissolve poorly in methanol at higher concentrations. Cella *et al.*, Campos *et al.*, Zheng *et al.* and Ohno *et al.* all directly cite Chen *et al.* when discussing functionalisation with PBASE [3]–[6]. Other groups using PBASE for graphene or carbon nanotube functionalisation do not explicitly reference Chen *et al.* in their methodology, but it is apparent they often draw on one of these two original methods. This common ancestry becomes apparent from the high frequency of methods detailing the use of 6 mM PBASE in DMF and 1 mM PBASE in methanol, as seen in Table 5.1.

However, despite this shared heritage, it is also apparent from Table 5.1 that there is a large degree of variation in the methods used for PBASE functionalisation. Various electrical characterisation, microscopy and spectroscopy techniques have been used to demonstrate successful functionalisation. However, there has historically been little justification provided for the exact parameters used in the procedure. As noted by Zhen *et al.* and Hinnemo *et al.*, there is more generally a lack of systematic research into formation of pyrene-derivative monolayers on graphene and other carbon nanomaterials, despite the wide use of this chemistry in the literature [7], [8].

We purchased PBASE from two suppliers, Sigma-Aldrich and Setareh Biotech. Sigma recommends DMF and methanol as suitable solvents for dissolving PBASE alongside chloroform and DMSO. Setareh Biotech indicates methanol can be used for dissolving PBASE. The two suppliers have conflicting information for suitable storage of PBASE, with Sigma recommending room temperature storage while Setareh Biotech recommends storage of -5 to -30°C and protection from light and moisture. Figure 5.2 compares the shapes of NMR spectra of PBASE from each supplier dissolved in DMSO, alongside a blank DMSO spectrum.

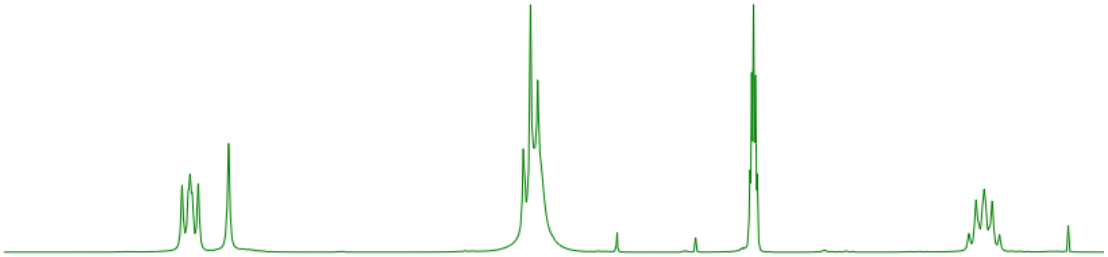

(a) Sigma PBASE in DMSO

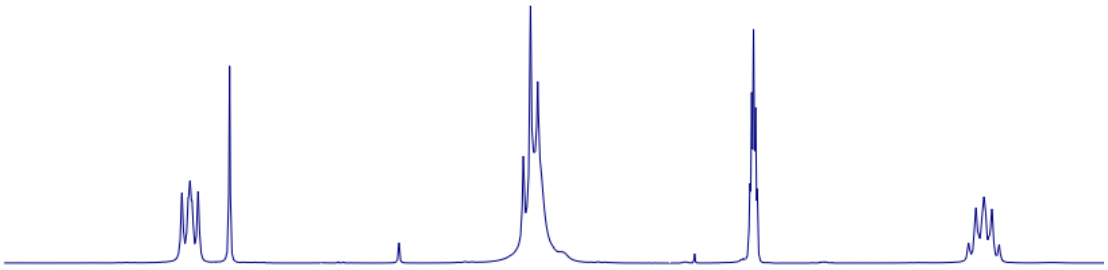

(b) Setareh PBASE in DMSO

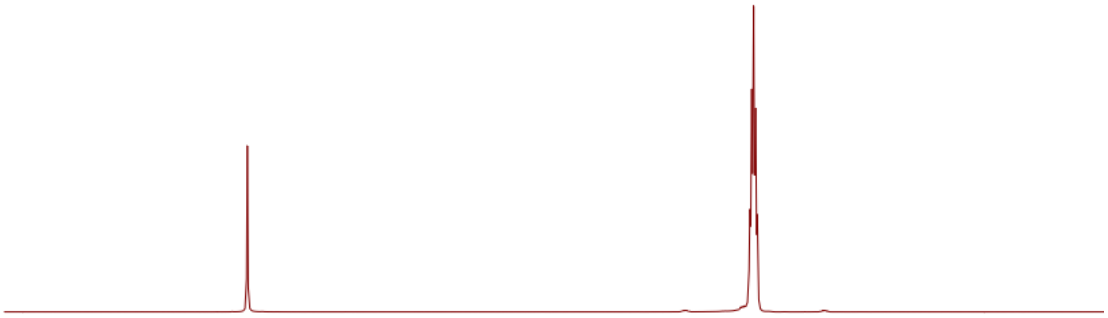

(c) Blank (DMSO only)

Figure 5.2.: Comparison of NMR spectrum profiles (arbitrary units)

Table 5.1.: Comparison of PBASE functionalisation processes used for immobilisation of proteins and aptamers onto liquid-gated CNTFET and graphene FET sensors

Solvent	Channel	Conc. (mM)	Incubation type	Time (hr)	Rinse steps	References
DMF	CNTs	5	Immersed	1	PBS	Maehashi *et al.* [9]
		6	Immersed	1	DMF, PBS	García-Aljaro *et al.* [10]
		6	Immersed	1	DMF	Chen *et al.* [2]
		6	Immersed	1	DMF	Cella *et al.* [3]
		6	Immersed	1	DMF	Das *et al.* [11]
	Graphene	-	-	2	DMF	Kwong Hong Tsang *et al.* [12]
		-	-	20	-	Wiedman *et al.* [13]
		0.2	Immersed	20	DMF, IPA, DI water	Gao *et al.* [14]
		1	100 μL droplet	6	DMF, IPA, DI water	Nekrasov *et al.* [15]
		5	Immersed	1	DMF, DI water	Hwang *et al.* [16]
		6	6 μL droplet	2	DMF, DI water	Nur Nasufiya *et al.* [17]
		10	10 μL droplet	2	DMF, DI water	Campos *et al.* [4]
		10	Immersed	2	DMF, PBS	Kuscu *et al.* [18]
		10	Immersed	1	DMF	Xu *et al.* [19]
		10	Immersed	12	DMF, ethanol, DI water	Khan *et al.* [20]
2-Methoxyethanol	Graphene	1	Immersed	1	DI water	Ono *et al.* [21]
Methanol	CNTs	1	Immersed	1	Methanol, DI water	Zheng *et al.* [5]
		1	Immersed	2	Methanol	Kim *et al.* [22]
	Graphene	5	Immersed	2	-	Sethi *et al.* [23]
		5	Immersed	1	Methanol, PBS	Ohno *et al.* [6]
DMSO	CNTs	10	-	1	DI water	Lopez *et al.* [24]
		10	Immersed	1	PBS	Strack *et al.* [25]

6. Results

What I found out.

See for more detailed results

7. Vapour Phase Sensing with Transistor Biosensors

7.1. Testing Vapour Delivery System

7.1.1. System Description

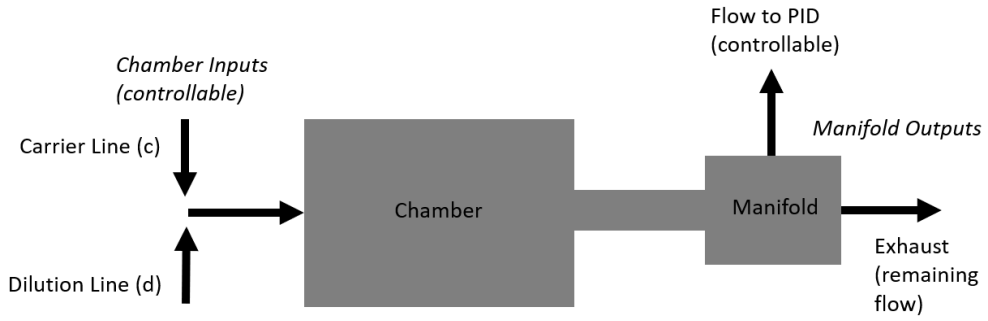

Figure 7.1.: Vapour Delivery System - Schematic of device chamber and manifold

7.1.2. Temperature and Humidity Indicator

7.1.3. Photoionisation Detector

Bubbling Vapour

First year report: “ ““First, a 200 sccm flow of N2 gas was sent through the dilution line to the device chamber until 1000 s. Then, the flow controller three-way valves were manually adjusted so that the same 200 sccm flow was directed through 50 mL of EtOH analyte in the carrier line. This continued until 2200 s, where the valves were again manually adjusted so that 200 sccm clean N2 again flowed through the device chamber. The resulting current across the device channel was monitored over this time, and is shown in Figure 19. A response to EtOH exposure and removal is visible.”“ ”

8. Summary

In summary, this book has no content whatsoever.

```
[1] 2
```

A. Photolithography

This section details some of the standard photolithography procedures used in the device fabrication processes detailed in Chapter 4. Photoresists, also referred to here as "resists", are UV light-sensitive polymeric resins used for photolithography. Photolithography procedures should be performed under yellow lighting, as light wavelengths from 320-450 nm can promote photo reactions in the photoresist used. Aging of photoresist over time can also significantly affect the photolithography process, and therefore all processes should be re-optimised regularly over time to give the desired result [26]. The range in processing times for some steps of the processes used here are largely due to the effects of aging on the photoresist.

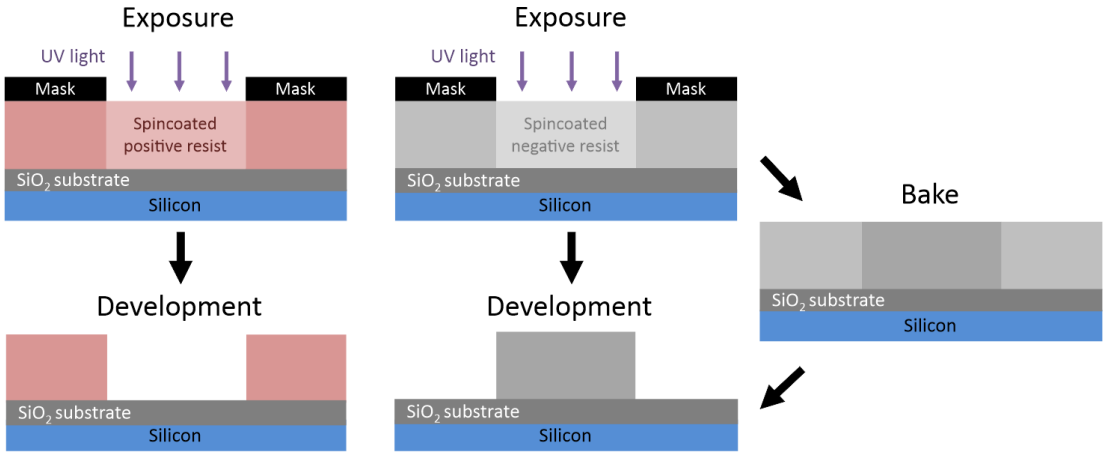

Figure A.1.: A side-view comparison of generic photolithography processes for positive and negative resists in the ideal case. Photolithography with a positive resist requires a single softbake step before exposure, while for negative resists a second baking step is required after exposure (Thicknesses shown not to scale).

Photolithography was performed using both positive and negative photoresists. Positive resists are made soluble in alkalines by UV light exposure, meaning exposed areas are removed in the development process. Conversely, negative resists are cross-linked by exposure and a post-exposure bake step. All photolithographic exposure was performed on a Karl Suss MJB3 Contact Aligner with a USHIO super-high pressure 350 W mercury lamp (USH-350DS, Japan). When performing lithography, the intensity reading from the aligner was 20.8 - 24.2 mW/cm^2 (Note however that an external photometer reading at

400 nm found an intensity output of 17.2 mW/cm^2 when the aligner read 21.0 mW/cm^2). The unexposed areas of the negative resist are then removed in the development process [26]. Figure A.1 gives a visual representation of these differences.

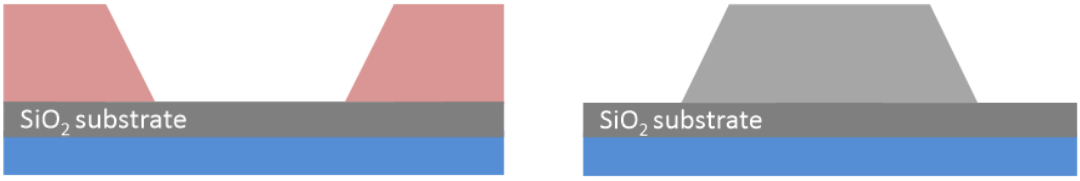

(a) Overcut profile of a positive resist

(b) Undercut profile of a negative resist

Figure A.2.: Two different resist profiles seen for different types of photoresist. The undercut profile is ideal for thin-film metal deposition and subsequent patterned removal, known as "lift-off".

The specific photoresist selected for photolithography depends on the specific use case. The types used in this thesis are positive and negative AZ® photoresists (AZ® 1518, Microchemicals GmbH; AZ® nLOF 2020, Microchemicals GmbH) and SU-8 (SU8-2150, Kayaku Advanced Materials, formerly Microchem). The AZ® resists used here have a minimum film thickness of 1.5 μm [26], while the SU8-2150 has a minimum film thickness of 0.5 μm [27]. Positive resists which have not been thermally crosslinked will soften at higher temperatures ($\gtrsim$ 100°C for AZ® 1518), leading to a rounded profile. This is not the case for negative resists, which are more thermally stable [26]. Each resist therefore has a different cross-section profile, as shown in Figure A.2.

The negative resist profile is more suited to metal or metal oxide deposition and lift-off processes [26], though the process is more sensitive to error due to the extrarequiring more processing steps than positive resist. Finally, when it is suitably processed SU-8 is considered to be more biocompatible than other photoresists. It is especially biocompatible when chemically modified via processes such as isopropanol sonication and O_2 plasma treatment [28].

The step-by-step processes for each resist are detailed in the subsequent sections.

A.1. AZ® 1518 photoresist

1. Spincoat at a final speed of 4000 rotations per minute (rpm) for 1 minute, with an initial acceleration of 500 rpm/s (notes: clean the substrate with acetone, isopropanol (IPA) and nitrogen before spincoating; use only the minimum amount of photoresist required to fully cover the wafer surface; avoid any gaps or bubbles in the photoresist). This gave
2. Softbake 2-4 minutes at 95°C on the hotplate (2 min for individual devices, 4 min for a quarter wafer)

3. Mask expose for 10-12 s (note: clean mask with acetone/IPA and N_2 dry before use)
4. Develop with 3 parts AZ® 326 (2.38 % TMAH metal-ion free developer, Microchemicals GmbH) in 1 part deionised (DI) water for 30-45 s (note: rinse for 10-15 s in one development solution, then perform the rest of the development in clean developer for a cleaner profile)
5. Rinse device for 30 s in DI water to remove excess developer, then dry under nitrogen

A.2. AZ® nLOF 2020 photoresist

1. Spincoat at final speed of 3000 rotations per minute (rpm) for 1 minute, with an initial acceleration of 500 rpm/s (notes: clean the substrate with acetone, isopropanol (IPA) and nitrogen before spincoating; avoid any gaps or bubbles in the photoresist)
2. Softbake for precisely 60 s at 110°C on the hotplate
3. Mask expose for 2.7-3 s (note: clean mask with acetone/IPA and N_2 dry before use)
4. Post-exposure bake for precisely 60 s at 110°C on the hotplate to cross-link exposed resist
5. Develop with 3 parts AZ® 326 in 1 part DI water for 60-70 s (note: rinse for 30 s in one development solution, then perform the rest of the development in clean developer for a cleaner profile)
6. Rinse device for 30 s in DI water to remove excess developer, then dry under nitrogen

A.3. SU8-2150 photoresist

1. SU-8 was diluted in cyclopentanone until viscosity was low enough to spincoat on substrate and then sonicated at 50°C for 3-4 hours (Note: The dilution ratio used was ~1 part SU-8 to 5 parts cyclopentanone. However, the age of the SU-8 may mean that significant evaporation had occurred prior to use, and the amount of SU-8 actually present is underrepresented by this ratio)
2. Spincoat first with a final speed of 500 rpm (acceleration 500 rpm/s) for 10 seconds, followed by spincoating at 4000 rpm (acceleration 7500 rpm/s) for 40 s.
3. Softbake for 10 minutes at 95°C on the hotplate

4. Mask expose for 6-8 s (note: clean mask with acetone/IPA and N_2 dry before use)
5. Post-exposure bake for 10 minutes at 95°C on the hotplate to cross-link exposed resist
6. Develop with SU-8 developer (Kayaku Advanced Materials, formerly Microchem) for 10-15 s, then clean in IPA for 30 s, repeat this step once then dry under nitrogen

B. Python Code for Data Analysis

C. Vapour Delivery System

C.1. Technical Notes

Two LabView Virtual Instruments (VIs) were adapted from pre-existing VIs for operating the mass flow controllers and monitoring vapour flow into the device chamber, as well as monitoring temperature and humidity in the vapour delivery system's manifold. These VIs were named " " A third VI was developed in parallel which combined the first two Virtual Instruments, alongside allowing the sequence of values to control the mass flow controllers.

From Honours report: " " " Figure 12 gives the right side of the front panel of the LabView VI sample with vapour.VI, which letsus preset an autonomously-performed vapour sensing sequence. Each row in each array module corresponds to a differennest step in this sequence. The 'howManySteps' module lets us set how many of these steps are performed. The 'Durations Array' module determines the length of time in seconds each step is performed over. The 'Carrier Flows Array' and 'Dilution Flows Array' modules let us set the carrier flow and dilution flow, respectively, in standard cubic centimetres per minute (sccm) through the gas rig at each step. The carrier flow pushes analyte vapour into the vapour-sensing device chamber, while dilution flow is used to modify the flow behaviour of the analyte vapour entering the chamber. The vapour sensing sequence as depicted in Figure 12 was used for all vapour sensing runs in this investigation. At the end of the sequence, the data collected about the vapour sensing process was saved as an .lvm file. " " "

C.2. Future Improvements

Bibliography

[1] J. A. M. J. Frisch and G. W. Trucks and H. B. Schlegel and G. E. Scuseria and M. A. Robb and J. R. Cheeseman and G. Scalmani and V. Barone and G. A. Petersson and H. Nakatsuji and X. Li and M. Caricato and A. V. Marenich and J. Bloino and B. G. Janesko and R. G, J. E. Peralta, F. Ogliaro, et al. *Gaussian˜16 Revision C.01*. 2016.

[2] R. J. Chen, Y. Zhang, D. Wang, et al. "Noncovalent sidewall functionalization of single-walled carbon nanotubes for protein immobilization". In: *Journal of the American Chemical Society* 123.16 (2001), pp. 3838–3839. ISSN: 00027863. DOI: 10.1021/ja010172b. URL: http://pubs.acs.org..

[3] Lakshmi N. Cella, Pablo Sanchez, Wenwan Zhong, et al. "Nano aptasensor for Protective Antigen Toxin of Anthrax". In: *Analytical Chemistry* 82.5 (Mar. 2010), pp. 2042–2047. ISSN: 00032700. DOI: 10.1021/ac902791q. URL: https://pubs.acs.org/doi/full/10.1021/ac902791q.

[4] Rui Campos, Jérôme Borme, Joana Rafaela Guerreiro, et al. "Attomolar label-free detection of dna hybridization with electrolyte-gated graphene field-effect transistors". In: *ACS Sensors* 4.2 (Feb. 2019), pp. 286–293. ISSN: 23793694. DOI: 10.1021/acssensors.8b00344. URL: https://pubs.acs.org/doi/full/10.1021/acssensors.8b00344.

[5] Han Yue Zheng, Omar A. Alsager, Bicheng Zhu, et al. "Electrostatic gating in carbon nanotube aptasensors". In: *Nanoscale* 8.28 (July 2016), pp. 13659–13668. ISSN: 20403372. DOI: 10.1039/c5nr08117c. URL: https://pubs.rsc.org/en/content/articlehtml/2016/nr/c5nr08117c%20https://pubs.rsc.org/en/content/articlelanding/2016/nr/c5nr08117c.

[6] Yasuhide Ohno, Kenzo Maehashi, and Kazuhiko Matsumoto. "Label-free biosensors based on aptamer-modified graphene field-effect transistors". In: *Journal of the American Chemical Society* 132.51 (Dec. 2010), pp. 18012–18013. ISSN: 00027863. DOI: 10.1021/ja108127r. URL: https://pubs.acs.org/doi/full/10.1021/ja108127r.

[7] Xue V. Zhen, Emily G. Swanson, Justin T. Nelson, et al. "Noncovalent monolayer modification of graphene using pyrene and cyclodextrin receptors for chemical sensing". In: *ACS Applied Nano Materials* 1.6 (June 2018), pp. 2718–2726. ISSN: 25740970. DOI: 10.1021/ACSANM.8B00420/ASSET/IMAGES/LARGE/AN-2018-00420J_0004.JPEG. URL: https://pubs.acs.org/doi/full/10.1021/acsanm.8b00420.

[8] Malkolm Hinnemo, Jie Zhao, Patrik Ahlberg, et al. "On Monolayer Formation of Pyrenebutyric Acid on Graphene". In: *Langmuir* 33.15 (Apr. 2017), pp. 3588–3593. ISSN: 15205827. DOI: 10.1021/ACS.LANGMUIR.6B04237/ASSET/IMAGES/LARGE/LA-2016-04237V_0003.JPEG. URL: https://pubs.acs.org/doi/full/10.1021/acs.langmuir.6b04237.

[9] Kenzo Maehashi, Taiji Katsura, Kagan Kerman, et al. "Label-free protein biosensor based on aptamer-modified carbon nanotube field-effect transistors". In: *Analytical Chemistry* 79.2 (Jan. 2007), pp. 782–787. ISSN: 00032700. DOI: 10.1021/ac060830g. URL: https://pubs.acs.org/doi/full/10.1021/ac060830g.

[10] Cristina García-Aljaro, Lakshmi N. Cella, Dhamanand J. Shirale, et al. "Carbon nanotubes-based chemiresistive biosensors for detection of microorganisms". In: *Biosensors and Bioelectronics* 26.4 (Dec. 2010), pp. 1437–1441. ISSN: 09565663. DOI: 10.1016/j.bios.2010.07.077.

[11] Basanta K. Das, Chaker Tlili, Sushmee Badhulika, et al. "Single-walled carbon nanotubes chemiresistor aptasensors for small molecules: Picomolar level detection of adenosine triphosphate". In: *Chemical Communications* 47.13 (Mar. 2011), pp. 3793–3795. ISSN: 1364548X. DOI: 10.1039/c0cc04733c. URL: https://pubs.rsc.org/en/content/articlehtml/2011/cc/c0cc04733c%20https://pubs.rsc.org/en/content/articlelanding/2011/cc/c0cc04733c.

[12] Deana Kwong Hong Tsang, Tyler J. Lieberthal, Clare Watts, et al. "Chemically Functionalised Graphene FET Biosensor for the Label-free Sensing of Exosomes". In: *Scientific Reports* 9.1 (Sept. 2019), pp. 1–10. ISSN: 20452322. DOI: 10.1038/s41598-019-50412-9. URL: https://www.nature.com/articles/s41598-019-50412-9.

[13] Gregory R. Wiedman, Yanan Zhao, Arkady Mustaev, et al. "An Aptamer-Based Biosensor for the Azole Class of Antifungal Drugs". In: *mSphere* 2.4 (Aug. 2017). ISSN: 23795042. DOI: 10.1128/msphere.00274-17. URL: /pmc/articles/PMC5566834/%20/pmc/articles/PMC5566834/?report=abstract%20https://www.ncbi.nlm.nih.gov/pmc/articles/PMC5566834/.

[14] Zhaoli Gao, Han Xia, Jonathan Zauberman, et al. "Detection of Sub-fM DNA with Target Recycling and Self-Assembly Amplification on Graphene Field-Effect Biosensors". In: *Nano Letters* 18.6 (June 2018), pp. 3509–3515. ISSN: 15306992. DOI: 10.1021/acs.nanolett.8b00572. URL: https://pubs.acs.org/doi/full/10.1021/acs.nanolett.8b00572.

[15] Nikita Nekrasov, Natalya Yakunina, Averyan V. Pushkarev, et al. "Spectral-phase interferometry detection of ochratoxin a via aptamer-functionalized graphene coated glass". In: *Nanomaterials* 11.1 (Jan. 2021), pp. 1–10. ISSN: 20794991. DOI: 10.3390/nano11010226. URL: https://www.mdpi.com/2079-4991/11/1/226/htm%20https://www.mdpi.com/2079-4991/11/1/226.

[16] Michael T. Hwang, B. Landon Preston, Lee Joon, et al. "Highly specific SNP detection using 2D graphene electronics and DNA strand displacement". In: *Proceedings of the National Academy of Sciences of the United States of America* 113.26 (June 2016), pp. 7088–7093. ISSN: 10916490. DOI: 10.1073/pnas.1603753113. URL: https://www.pnas.org/doi/abs/10.1073/pnas.1603753113.

[17] Mohd Maidin Nur Nasyifa, A. Rahim Ruslinda, Nur Hamidah Abdul Halim, et al. "Immuno-probed graphene nanoplatelets on electrolyte-gated field-effect transistor for stable cortisol quantification in serum". In: *Journal of the Taiwan Institute of Chemical Engineers* 117 (Dec. 2020), pp. 10–18. ISSN: 18761070. DOI: 10.1016/j.jtice.2020.12.008.

[18] Murat Kuscu, Hamideh Ramezani, Ergin Dinc, et al. "Graphene-based Nanoscale Molecular Communication Receiver: Fabrication and Microfluidic Analysis". In: (June 2020). arXiv: 2006.15470. URL: https://arxiv.org/abs/2006.15470v2.

[19] Shicai Xu, Jian Zhan, Baoyuan Man, et al. "Real-time reliable determination of binding kinetics of DNA hybridization using a multi-channel graphene biosensor". In: *Nature Communications* 8.1 (Mar. 2017), pp. 1–10. ISSN: 20411723. DOI: 10.1038/ncomms14902. URL: https://www.nature.com/articles/ncomms14902.

[20] Niazul I. Khan, Mohammad Mousazadehkasin, Sujoy Ghosh, et al. "An integrated microfluidic platform for selective and real-time detection of thrombin biomarkers using a graphene FET". In: *Analyst* 145.13 (June 2020), pp. 4494–4503. ISSN: 13645528. DOI: 10.1039/d0an00251h. URL: https://pubs.rsc.org/en/content/articlehtml/2020/an/d0an00251h%20https://pubs.rsc.org/en/content/articlelanding/2020/an/d0an00251h.

[21] T Ono, K Kamada, R Hayashi, et al. "Lab-on-a-graphene-FET detection of key molecular events underpinning influenza 2 virus infection and effect of antiviral drugs 3 Running title: Graphene-FET detects reactions in an influenza infection MAIN TEXT". In: *bioRxiv* (Mar. 2020), p. 2020.03.18.996884. DOI: 10.1101/2020.03.18.996884. URL: https://doi.org/10.1101/2020.03.18.996884.

[22] Jun Pyo Kim, Byung Yang Lee, Joohyung Lee, et al. "Enhancement of sensitivity and specificity by surface modification of carbon nanotubes in diagnosis of prostate cancer based on carbon nanotube field effect transistors". In: *Biosensors and Bioelectronics* 24.11 (July 2009), pp. 3372–3378. ISSN: 09565663. DOI: 10.1016/j.bios.2009.04.048. URL: https://pubmed.ncbi.nlm.nih.gov/19481922/.

[23] Jagriti Sethi, Michiel Van Bulck, Ahmed Suhail, et al. "A label-free biosensor based on graphene and reduced graphene oxide dual-layer for electrochemical determination of beta-amyloid biomarkers". In: *Microchimica Acta* 187.5 (May 2020), pp. 1–10. ISSN: 14365073. DOI: 10.1007/s00604-020-04267-x. URL: https://link.springer.com/article/10.1007/s00604-020-04267-x.

[24] Ryan J. Lopez, Sofia Babanova, Kateryna Artyushkova, et al. "Surface modifications for enhanced enzyme immobilization and improved electron transfer of PQQ-dependent glucose dehydrogenase anodes". In: *Bioelectrochemistry* 105 (Oct. 2015), pp. 78–87. ISSN: 1878562X. DOI: 10.1016/j.bioelechem.2015.05.010. URL: https://pubmed.ncbi.nlm.nih.gov/26011132/.

[25] Guinevere Strack, Robert Nichols, Plamen Atanassov, et al. "Modification of carbon nanotube electrodes with 1-pyrenebutanoic acid, succinimidyl ester for enhanced bioelectrocatalysis". In: *Methods in Molecular Biology* 1051 (2013), pp. 217–228. ISSN: 10643745. DOI: 10.1007/978-1-62703-550-7_14. URL: https://pubmed.ncbi.nlm.nih.gov/23934807/.

[26] MicroChemicals. *Photoresists AZ and MicroChemicals TI resists*. URL: https://www.microchemicals.com/products/photoresists.html (visited on 2023-06-09).

[27] *SU-8 2000 Permanent Negative Epoxy Photoresist | Kayaku*. URL: https://kayakuam.com/products/su-8-2000/ (visited on 2023-06-30).

[28] Ziyu Chen and Jeong Bong Lee. "Biocompatibility of SU-8 and Its Biomedical Device Applications". In: *Micromachines 2021, Vol. 12, Page 794* 12.7 (July 2021), p. 794. ISSN: 2072-666X. DOI: 10.3390/MI12070794. URL: https://www.mdpi.com/2072-666X/12/7/794/htm%20https://www.mdpi.com/2072-666X/12/7/794.